Chem Soc Rev

TUTORIAL REVIEW

View Article Online
View Journal | View Issue

Published on 13 January 2014. Downloaded by Indian Institute of Technology Chennai on 07/02/2017 06:22:37.

Cite this: *Chem. Soc. Rev.*, 2014, **43**, 7520

Recent advances in semiconductors for photocatalytic and photoelectrochemical water splitting

Takashi Hisatomi, Jun Kubota and Kazunari Domen*

Photocatalytic and photoelectrochemical water splitting under irradiation by sunlight has received much attention for production of renewable hydrogen from water on a large scale. Many challenges still remain in improving energy conversion efficiency, such as utilizing longer-wavelength photons for hydrogen production, enhancing the reaction efficiency at any given wavelength, and increasing the lifetime of the semiconductor materials. This introductory review covers the fundamental aspects of photocatalytic and photoelectrochemical water splitting. Controlling the semiconducting properties of photocatalysts and photoelectrode materials is the primary concern in developing materials for solar water splitting, because they determine how much photoexcitation occurs in a semiconductor under solar illumination and how many photoexcited carriers reach the surface where water splitting takes place. Given a specific semiconductor material, surface modifications are important not only to activate the semiconductor for water splitting but also to facilitate charge separation and to upgrade the stability of the material under photoexcitation. In addition, reducing resistance loss and forming p–n junction have a significant impact on the efficiency of photoelectrochemical water splitting. Correct evaluation of the photocatalytic and photoelectrochemical activity for water splitting is becoming more important in enabling an accurate comparison of a number of studies based on different systems. In the latter part, recent advances in the water splitting reaction under visible light will be presented with a focus on non-oxide semiconductor materials to give an overview of the various problems and solutions.

Received 24th October 2013

DOI: 10.1039/c3cs60378d

www.rsc.org/csr

Key learning points

- Behaviour of photoexcited carriers during photocatalytic and photoelectrochemical water splitting from a thermodynamic perspective.
- Design concept of non-oxide semiconductors for visible-light-driven water splitting.
- Criteria for evaluating the photocatalytic and photoelectrochemical activity for water splitting.
- Case studies on the effect of cocatalyst loading, reaction conditions, surface modifications, and advanced electrode fabrication on photocatalytic and photoelectrochemical water splitting, taken from recent research.

1. Introduction

Efficient utilization of solar energy could alleviate many energy and environmental issues, as the solar energy irradiating the surface of the Earth (1.3×10^5 TW) exceeds the current global human energy consumption (1.6×10^1 TW in 2010[1]) by roughly four orders of magnitude. Overall water splitting under sunlight has received much attention for production of renewable hydrogen from water on a large scale.[2–4] Since the discovery of the Honda–Fujishima effect in the early 1970s, which demonstrated photo-assisted electrochemical water oxidation on an n-type TiO single-crystal electrode by band-gap excitation,[5] photocatalytic and photoelectrochemical (PEC) water splitting on semiconducting materials has been studied extensively. Solar hydrogen will play an important role in prospective sustainable-energy societies because it is storable, transportable and can be converted into electricity efficiently using fuel cells whenever it is necessary. Moreover, hydrogen is applicable as feedstock in the modern chemical industry and could be used for recycling of carbon dioxide *via* chemical processes such as the Fischer–Tropsch reaction and methanol synthesis.

Department of Chemical System Engineering, School of Engineering, The University of Tokyo, 7-3-1 Hongo, Bunkyo-ku, 113-8656 Tokyo, Japan.
E-mail: domen@chemsys.t.u-tokyo.ac.jp; Fax: +81-3-5841-8838;
Tel: +81-3-5841-1148

This journal is © The Royal Society of Chemistry 2014

Published on 13 January 2014. Downloaded by Indian Institute of Technology Chennai on 07/02/2017 06:22:37.

The water splitting reaction is an uphill reaction in which the Gibbs free energy increases by 237 kJ mol^{-1}. The energy needed to drive photocatalytic and PEC water splitting is provided by light or ideally sunlight. Fig. 1 shows the schematic of the reaction processes of photocatalytic water splitting.[6] Electrons and holes are generated inside semiconductor photocatalyst particles by band-gap excitation. Photoexcited carriers are transferred to surface active sites and subsequently consumed by surface redox reactions. Mass diffusion of reactants and products should proceed concurrently. Recombination of photoexcited carriers occurs along with these reactions. Therefore, the charge separation in photocatalyst particles and the redox reactions on their surface must proceed within the lifetimes of photoexcited carriers for successful water splitting. Note that, in many cases, recombination is the main process that photoexcited carriers undergo. In order to facilitate the charge separation and surface reaction, photocatalysts and photoelectrodes are modified with appropriate cocatalysts and buffer layers.

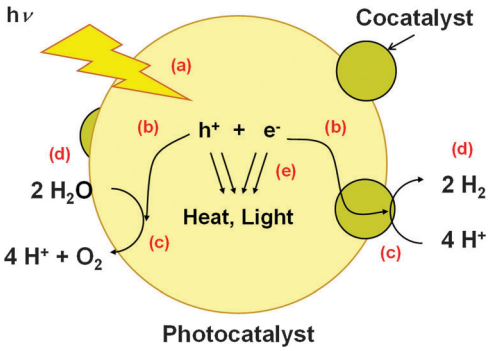

Fig. 1 Reaction processes of water splitting on a heterogeneous photocatalyst. (a) Light absorption, (b) charge transfer, (c) redox reactions, (d) adsorption, desorption, and mass diffusion of chemical species, and (e) charge recombination.[6] ©2012 The Chemical Society of Japan.

This review covers the fundamental aspects of photocatalytic and PEC water splitting under visible light, focusing on non-oxide semiconductor materials. First, the behaviour of photoexcited carriers during photocatalytic and PEC water splitting is described on the basis of thermodynamics to provide an overview of the working principle of the reactions. Secondly, the design concept of non-oxide materials for visible-light-driven water splitting is reviewed. Then, criteria for evaluating photocatalytic and PEC activity for water splitting are presented, along with technical remarks. Finally, recent advances in photocatalytic and PEC water splitting under visible light are described in the context of cocatalyst loading, reaction conditions, surface modifications, and electrode fabrication processes. Informative review articles on solar hydrogen production have been published, featuring reaction systems,[7,8] extensive material development,[3,4,9–11] selected promising materials,[12,13] nanostructuring,[14] and

Takashi Hisatomi

Takashi Hisatomi received his PhD in Engineering from the University of Tokyo under Prof. Dr Domen's supervision in March 2010. He joined Laboratory of Photonics and Interfaces in École Polytechnique Fédérale de Lausanne led by Prof. Dr Grätzel in April 2010 for two years as a postdoctoral fellow. He has been studying in Prof. Dr Domen's laboratory in the University of Tokyo since April 2012 and works as an assistant professor currently. His major research interests are material development and device design for photocatalytic and photoelectrochemical water splitting using solar energy as well as kinetic assessments of photocatalysis and photoelectrochemistry.

Jun Kubota

Associate Prof. Jun Kubota received his PhD in Tokyo Institute of Technology in March 1995. He had worked as an assistant professor in Tokyo Institute of Technology until 2007 and was promoted to Associate Professor of the University of Tokyo in 2007. He is interested in surface chemistry, catalysis, and electrochemistry on the basis of physicochemical methods such as vibrational spectroscopies. His recent research interests are inclined to electrocatalysts for fuel cells and photocatalytic and photoelectrochemical water splitting. He has published more than 100 peer-reviewed papers in international academic journals.

Kazunari Domen

Prof. Kazunari Domen received BSc (1976), MSc (1979), and PhD (1982) honors in chemistry from the University of Tokyo. Dr Domen joined Chemical Resources Laboratory, Tokyo Institute of Technology, in 1982 as Assistant Professor and was promoted to Associate Professor in 1990 and Professor in 1996, having moved to the University of Tokyo as Professor in 2004. Domen has been working on overall water splitting reaction on heterogeneous photocatalysts to generate clean and recyclable hydrogen. His research interests now include heterogeneous catalysis and materials chemistry, with particular focus on surface chemical reaction dynamics, photocatalysis, solid acid catalysis, and mesoporous materials.

Published on 13 January 2014. Downloaded by Indian Institute of Technology Chennai on 07/02/2017 06:22:37.

kinetic aspects.[6] Readers are encouraged to consult these references.

2. Thermodynamics of photocatalytic and photoelectrochemical water splitting

When a semiconductor absorbs photons with energies higher than its band gap energy, electrons in the valence band are excited to the conduction band. As a result, excited electrons and holes are generated in the conduction and valence bands, respectively. These photogenerated carriers can drive reduction and oxidation reactions if the charge injections into the reactants are thermodynamically favourable. To achieve photocatalytic water splitting using a single photocatalyst, the band gap of the semiconductor must straddle the reduction and oxidation potentials of water, which are +0 and +1.23 V *vs.* normal hydrogen electrode (NHE), respectively, when the reactant solution is at pH 0, as shown in Fig. 2a. This is the principle of one-step water splitting.

Alternatively, two semiconductors can be connected in series with reversible redox shuttles (Fig. 2b). In this scheme, the reduction of water to hydrogen and oxidation of reduced redox mediators occur on one photocatalyst concurrently with the reduction of oxidized redox mediators and oxidation of water to oxygen on the other photocatalyst. This two-step photocatalytic system is called the "Z-scheme" after photosynthesis in green plants because of the similarity in the excitation and transfer processes of photoexcited electrons.[8] Z-scheme water splitting proceeds even in the absence of reversible redox shuttles in some cases because of the interparticle electron transfer during the physical contact between the hydrogen and oxygen evolution photocatalysts.

When a semiconductor electrode is immersed in an electrolyte solution, electron transfer takes place between the semiconductor and the electrolyte solution so that the Fermi level is equilibrated with the redox potential of electrolyte solution.[15] An electrolyte solution accepts (donates) electrons from (to) a semiconductor when the Fermi level of the semiconductor is more negative (positive) than the reduction potential of the electrolyte solution. Since the density of electrons in a semiconductor is

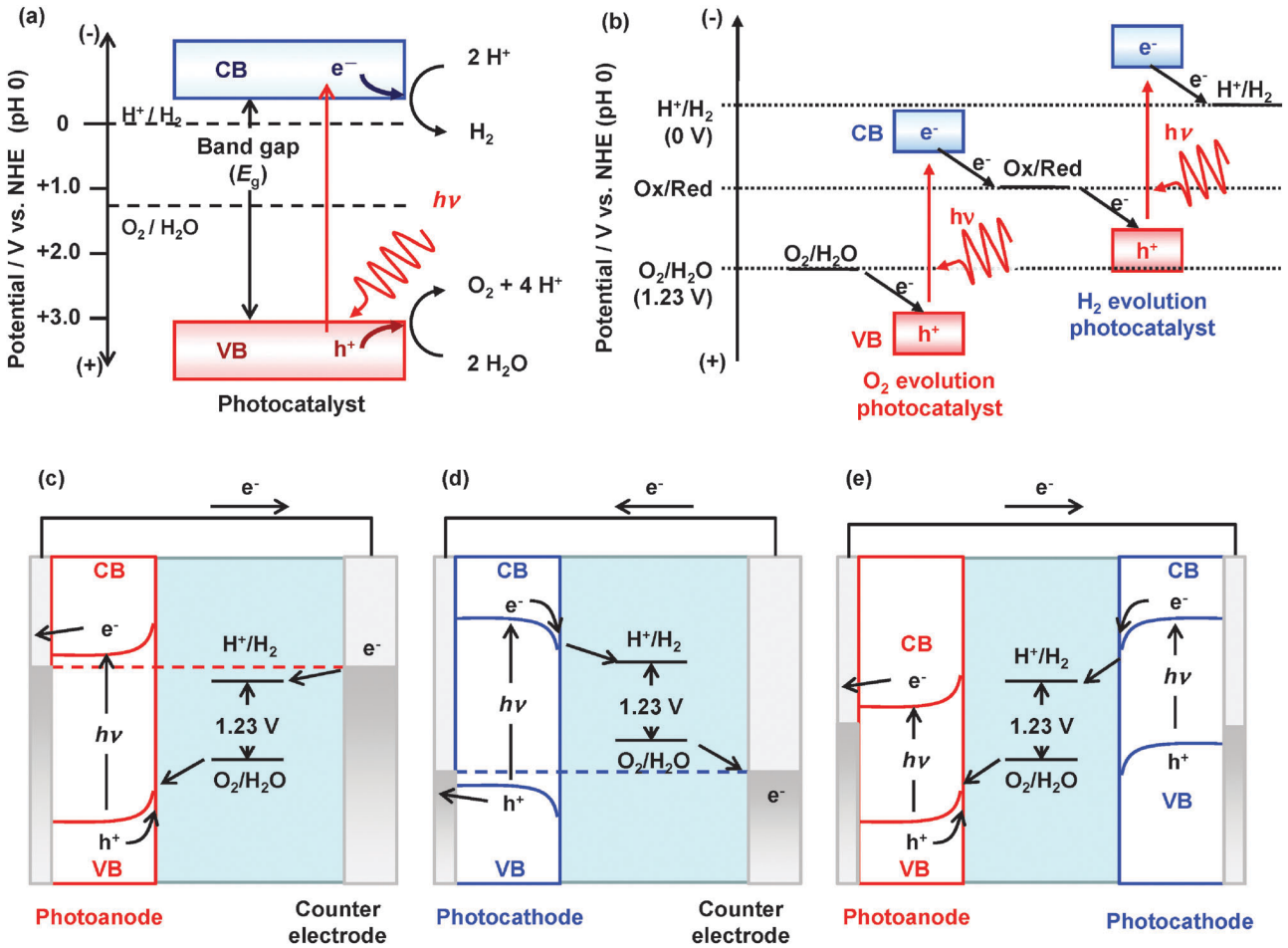

Fig. 2 Energy diagrams of photocatalytic water splitting based on (a) one-step excitation and (b) two-step excitation (Z-scheme); and PEC water splitting using (c) a photoanode, (d) photocathode, and (e) photoanode and photocathode in tandem configuration. The band gaps are depicted smaller in (b) and (e) to emphasize that semiconductors with a narrow band gap can be employed.

 This journal is © The Royal Society of Chemistry 2014

Published on 13 January 2014. Downloaded by Indian Institute of Technology Chennai on 07/02/2017 06:22:37.

finite and the potentials of the band positions at the interfaces can be assumed to be pinned, the electron transfer causes band bending. Note that band bending could also occur in semiconductor particles suspended in an aqueous solution, although its effect might be less pronounced for nanoparticles in which the width of the space charge layer could be larger than the particle sizes. The electric field induced by the space charge layer plays an important role in charge separation.[15] In electrodes of n-type semiconductors, which act as photoanodes, photoexcited holes accumulate on the surface of the semiconductor and are consumed in oxidation reactions, while electrons are transferred to a counter electrode *via* the back contact and an external circuit, and used in reduction reactions, as shown in Fig. 2c. The top of the valence band must be more positive than the oxygen evolution potential to allow a photoanode to generate oxygen. On the other hand, a p-type semiconductor works as a photocathode for hydrogen evolution when the conduction band edge is more negative than the hydrogen evolution potential as shown in Fig. 2d. Accordingly, PEC reactions on photoelectrodes are driven by photoexcited minority carriers in both cases. The potential of electrons on the counter electrode is identical to the Fermi level of the photoelectrode under photoexcitation. An external voltage can be applied between a photoelectrode and a counter electrode to compensate for the potential deficiency in order to drive redox reactions on a counter electrode even if the Fermi level of the photoelectrode is positioned at an undesirable potential. In such a case, the external power input, which is the product of the current and the applied voltage, should be subtracted from the energy output when the energy conversion efficiency is considered.[7] Alternatively, a photoanode and a photocathode can be connected in tandem as in Z-scheme water splitting (see Fig. 2e) instead of using a single photoelectrode and a counter electrode. In the tandem configuration, the maximum photocurrent and the working potential of the photoelectrodes are theoretically determined by the intersection of the steady current–potential curves of the respective photoelectrodes.[3]

3. Development of non-oxide photocatalysts for visible-light-driven photocatalysis

Sunlight (AM1.5G) consists of three main components in terms of wavelengths: ultraviolet (UV) rays ($\lambda < 400$ nm), visible light (400 nm $< \lambda <$ 800 nm), and infrared rays ($\lambda > 800$ nm), accounting for 4, 53, and 43% of the total solar energy, respectively. The theoretical maximum efficiency of solar energy conversion using a single photocatalyst increases with the wavelength available for the water splitting reaction, calculated to be 2, 16, and 32% when solar light between UV and, respectively, 400, 600, and 800 nm is utilized at a quantum efficiency of 100%.[2] It is necessary to harvest visible light for effective solar-to-hydrogen conversion because UV light accounts for only a small portion of solar energy.

Generally, photocatalytic materials for overall water splitting contain metal cations with d^0 and d^{10} electronic configurations at the highest oxidation states.[4,9] The conduction band of transition metal oxides with a d^0 electronic configuration mainly consists of the empty d orbitals of the constituent transition metal cations, while that of typical metal oxides with a d^{10} electronic configuration consists of hybridized orbitals of empty s and p orbitals of cations. On the other hand, the valence band of metal oxides is mainly composed of an O 2p orbital. Oxide photocatalysts that are active for overall water splitting such as $SrTiO_3$ have a band gap energy that is too large to absorb visible light. As the valence bands consisting of O 2p orbitals are located around +3 V *vs.* NHE (pH 0), the band gap energy inevitably exceeds the 3 eV needed to satisfy the thermodynamic requirement for water splitting that the band gap straddles the potentials of water reduction and oxidation. WO_3, $BiVO_4$, and Fe_2O_3 cannot produce hydrogen on the surface even after absorbing visible light because their conduction band edges are more positive than the hydrogen evolution potential. To accomplish water splitting using such oxides, additional semiconducting materials and an electric power supply are needed as in Z-scheme photocatalysis and PEC water splitting, respectively.

The present authors have studied (oxy)nitrides and oxysulphides for water splitting under visible light irradiation.[9] N 2p and S 3p orbitals of (oxy)nitrides and oxysulphides can form a valence band at potentials more negative than a band composed of O 2p orbitals, owing to the lower electronegativities of nitrogen and sulphur compared to oxygen, while the potential of the conduction band is largely unaffected by nitrogen and sulphur. In fact, certain (oxy)nitrides and oxysulphides have ideal band structures for overall water splitting: a band gap energy small enough to absorb visible light and a band gap straddling the reduction and oxidation potentials of water. Note that oxides doped with transition metals also absorb visible light through the excitation of impurity levels.[4] It has been demonstrated that some doped oxide photocatalysts can split water under visible light irradiation in Z-scheme systems.[16–18] Additionally, some chalcogenides containing Cu^I ions, such as $CuGaSe_2$,[19] Cu_2ZnSnS_4,[20,21] and $Cu(Ga,In)(S,Se)_2$, function as p-type semiconductors and can also be employed as photovoltaic cells. These p-type chalcogenides are not applicable to the water oxidation reaction because of photocorrosion and their valence band potential is insufficient for oxidizing water under typical reaction conditions. However, they are applicable to hydrogen evolution under potential control because reduction reactions predominantly occur on a p-type photocathode as presented in the previous section.

Band structures of Ta_2O_5, TaON, and Ta_3N_5 are shown in Fig. 3.[22] During the nitridation process, the three O^{2-} anions in the precursor Ta_2O_5 are replaced by two N^{3-} anions, whereas the valence state of Ta^{5+} is maintained. The top of the valence band of Ta_2O_5 consists of O 2p orbitals, which is located at *ca.* +3.4 V *vs.* NHE. In contrast, the N 2p orbitals of TaON and Ta_3N_5 are incorporated in the valence bands, shifting the top of the valence bands to *ca.* +2.0 V *vs.* NHE for TaON and +1.5 V *vs.*

Published on 13 January 2014. Downloaded by Indian Institute of Technology Chennai on 07/02/2017 06:22:37.

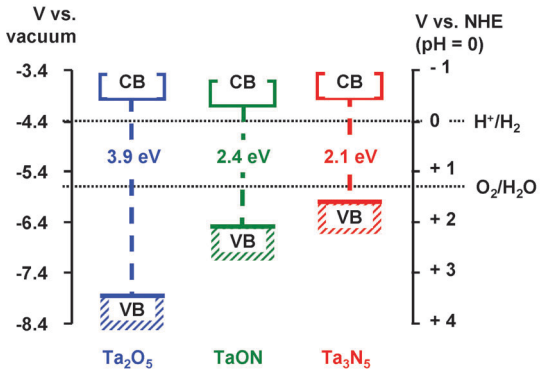

Fig. 3 Band structures of Ta_2O_5, TaON, and Ta_3N_5. Adapted with permission from ref. 22. ©2003 American Chemical Society.

NHE for Ta_3N_5. The conduction bands of the three Ta compounds mainly consist of empty Ta 5d orbitals and are located at comparable potentials, −0.3 to −0.5 V *vs.* NHE. Consequently, the light absorption spectra of TaON and Ta_3N_5 are expanded up to *ca.* 500 and 600 nm, respectively. Therefore, the nitrided products TaON and Ta_3N_5 have suitable band gap positions for photocatalytic water splitting although light absorption by Ta_2O_5 is limited in the UV region.

(Oxy)nitrides can be prepared by nitriding metal oxides with appropriate compositions under an NH_3 flow at high temperatures.[10] For example, TaON and Ta_3N_5 can be prepared by nitriding Ta_2O_5 under different nitridation conditions. Thermodynamically, NH_3 dissociates into H_2 and N_2 at elevated temperatures. However, the dissociation of NH_3 does not reach equilibrium when NH_3 gas flows continuously, and the concentration of NH_3 could be higher than the equilibrium value. Consequently, radical species such as NH and NH_2 are supplied to the precursor.[23] The activity of nitriding species generated by NH_3 dissociation increases as the nitridation temperature and the NH_3 flow rate increase.[24] Similarly, (oxy)sulphides can be prepared by sulphurizing metal films or metal oxides under a H_2S flow at elevated temperatures. For example, $Sm_2Ti_2S_2O_5$ powder[25] and Cu_2ZnSnS_4 layers[20] can be prepared by sulphurizing amorphous SmTi-oxide powder and Zn/Sn/Cu multilayers electroplated on Mo. Note that thermal nitridation and sulphurization of oxides under NH_3 and H_2S flows are non-equilibrium processes. Excessive reactions would lead to the thermal decomposition and/or reduction of desired semiconducting products as a result of the hydrogen generated by the dissociation of NH_3 and H_2S. Thus, the nitridation and sulphurization conditions need to be carefully fine-tuned to obtain active semiconducting materials. (Oxy)sulphides can also be prepared by the solid-state reactions of metal oxides and sulphides in a sealed vacuum tube. This process does not require elaborate setups, while careful control of impurities such as adsorbed water and hydrolysed sulphides is needed. High-quality chalcogenide thin films can also be fabricated through vacuum processes such as molecular beam epitaxy[26] and multi-source co-evaporation. Such processes prevail not only in high-efficiency photovoltaic cells but in PEC water splitting, owing to the similarity in the working mechanism.

4. Measurement of activity for water splitting

a. Apparatus

Photocatalytic water splitting reactions are usually carried out in a closed-circulation system equipped with a vacuum system or a flow system at atmospheric pressure. In a reaction using a closed-circulation system, a photocatalyst sample is dispersed in a reaction solution, and the reaction system is evacuated adequately to eliminate the dissolved air in the reaction solution. A certain amount of inert gas is introduced into the reaction system to keep the gas composition homogeneous by circulation and avoid boiling of the reaction solution under illumination at a reduced pressure. Alternatively, an open flow system is used for photocatalytic water splitting, where an inert gas flows continuously through the headspace of a reactor. In both cases, gaseous products are analysed using a gas chromatograph integrated with the reaction system to avoid air contamination. In practice, the pressure inside the reaction system affects the photocatalytic activity.[27] At a high pressure, the photocatalytic activity for overall water splitting generally decreases because of slower bubble formation and desorption of product gases, inducing side reactions such as oxygen reduction and water formation from the produced hydrogen and oxygen. These side reactions are critical problems in view of the practical operation of solar water splitting at ambient pressure. A hydrogen evolution cocatalyst that is highly selective for the desired reaction, such as $Rh_{2-y}Cr_yO_3$[27] or an Rh/Cr_2O_3 core/shell composite,[28] is needed.

PEC water splitting is performed using a single- or double-compartment cell equipped with a flat optical window.[7] The PEC cell has several ports for electrodes, purging, and gas sampling. Two-electrode and three-electrode systems are used to measure the efficiency of a whole cell and the performance of a working electrode as a half cell, respectively. In a two-electrode system, the photo- and dark-currents are recorded as a function of voltage against a counter electrode. The potential of the counter electrode is ideally the same as the potential of the redox reaction occurring on the counter electrode. However, in reality, the potential of the counter electrode is not at the equilibrium potential of the redox reaction because of the reaction overpotential, which in turn depends on the current density. Thus, the current–voltage curves are affected by the properties of the counter electrode. Consequently, the potential of the working electrode cannot be measured exactly in the simple two-electrode configuration. The purpose of the two-electrode measurement is to assess the efficiency of a PEC cell taking overpotential loss in both working and counter electrodes into account.

In a three-electrode system, the potential of a working electrode is controlled using a potentiostat with respect to a reference electrode. The photo- and dark-currents are recorded

 This journal is © The Royal Society of Chemistry 2014

Published on 13 January 2014. Downloaded by Indian Institute of Technology Chennai on 07/02/2017 06:22:37.

as a function of the potential against the electrolyte solution. It should be noted that the potential of the counter electrode is adjusted so that the current passing through the counter electrode matches that generated on the working electrode. Therefore, the efficiency of PEC cells could not be assessed from three-electrode measurements. The purpose of the three-electrode system is to define the potential of the working electrode against the electrolyte solution, which is independent of the properties of the counter electrode. The silver/silver chloride electrode, the saturated calomel electrode, and the mercury/mercury oxide electrode are commonly used in PEC water splitting. These reference electrodes can indicate the known potentials with respect to electrolyte solutions with different redox species, temperatures, and concentrations. The potential of the working electrode measured with respect to a reference electrode can be converted to the potential *vs.* the reversible hydrogen electrode (RHE) on the basis of the following equation:

$$E_{\mathrm{RHE}} = E_{\mathrm{ref}} + E^{0}_{\mathrm{ref}} + \frac{RT\ln 10}{F}\mathrm{pH}, \qquad (1)$$

where E_{RHE}, E_{ref}, and E^{0}_{ref} denote, respectively, the potential of the working electrode against the electrolyte solution with respect to the RHE, the potential of the working electrode measured with respect to a reference electrode, and the potential of the reference electrode with respect to the normal hydrogen electrode (NHE), if the potential of the reference electrode used is independent of pH. R, T, and F stand for the gas constant, temperature, and Faraday constant, respectively. The potentials at 0 and +1.23 V *vs.* RHE indicate the potentials where hydrogen and oxygen are equilibrated with the actual electrolyte solution.

Various kinds of light sources are used for illumination, including Hg lamps, Xe lamps, halogen lamps, and light-emitting diodes. Hg lamps and light-emitting diodes excel in generating emission line spectra, while Xe and halogen lamps mostly generate continuous spectra. Xe lamps equipped with appropriate filters can be used as a solar simulator. One must be careful of the power spectra (*i.e.*, intensity at different wavelengths) of a light source at different distances, positions, and times, because the photon and energy fluxes are important in the evaluation of quantum efficiencies and energy conversion efficiencies, respectively. In addition, heating of the reaction solution under illumination should be avoided because the water splitting rate depends on the reaction temperature.[6] Furthermore, fluctuations in vapour pressure could cause an inhomogeneity in the gaseous components in the reactor.

b. Efficiency

The benchmark efficiency of solar hydrogen production *via* water splitting and diagnostic efficiencies to understand material performance were reviewed recently.[7] The solar-to-hydrogen efficiency (STH) can be calculated from the product of the rate of hydrogen production ($r_{\mathrm{H_2}}$) and the gain in Gibbs energy (ΔG) of 237 kJ mol^{-1}:[4,7]

$$\mathrm{STH} = \frac{\text{Output energy as } \mathrm{H_2}}{\text{Energy of incident solar light}} = \frac{r_{\mathrm{H_2}} \times \Delta G}{P_{\mathrm{sun}} \times S}, \qquad (2)$$

where P_{sun} is the energy flux of the sunlight and S is the area of the reactor. Considering the ASTM-G173 AM1.5 global tilt, solar irradiation has an energy flux of 1.0×10^{3} W m^{-2} and its power spectrum is well defined.

When an external voltage is applied to PEC systems, the electrical energy has to be subtracted from the energy gain. For two-electrode measurements, the applied bias photon-to-current efficiency (ABPE) is frequently used.[7] ABPE is defined as

$$\mathrm{ABPE} = \frac{|j| \times (V_{\mathrm{th}} - V_{\mathrm{bias}})}{P_{\mathrm{sun}}}, \qquad (3)$$

where j, V_{th}, and V_{bias} are the photocurrent density, the theoretical water-electrolysis voltage (1.23 V), and the applied voltage, respectively. One of the concerns regarding ABPE as an alternative expression of STH is that the faradaic efficiency (η_{F}) is not considered explicitly.[7] Thus, the photocurrent is not necessarily attributed to water splitting unless the production of hydrogen and oxygen is confirmed at the faradaic efficiency of unity. The faradaic efficiency of water splitting is the ratio of the current contributing to water splitting into hydrogen and oxygen to the observed current. In the ideal scenario, four electrons correspond to two hydrogen molecules and one oxygen molecule. If the faradaic efficiency is below unity, a part of the current should be attributed to redox processes other than water splitting.

Considering the ambiguous definition and naming of ABPE either as energy conversion efficiency or quantum efficiency, we suggest applied-bias-compensated solar-to-hydrogen efficiency (AB-STH) as a general expression of STH *via* PEC water splitting under sunlight:

$$\text{AB-STH} = \frac{|j| \times \eta_{\mathrm{F}} \times (V_{\mathrm{th}} - V_{\mathrm{bias}})}{P_{\mathrm{sun}}}. \qquad (4)$$

STH in eqn (2) corresponds to a special case of AB-STH such that η_{F} is unity and V_{bias} is zero. It should be noted that current–voltage curves often have a significant hysteresis in cyclic voltammetry because of charging/decharging of trap states, cocatalysts, and the surface of photoelectrodes. To get an accurate estimate of AB-STH, it is necessary to employ a two-electrode system and measure the photocurrent at a static applied voltage. It is obviously necessary to quantify the amounts of evolved H_2 and O_2 because η_{F} must be known. PEC cells should be purged with an inert gas when side reactions involving oxygen and hydrogen are a concern. Moreover, even if the value of AB-STH is high, the performance is considered to be low when the potential gain is much smaller than 1.23 V. Such systems split water mostly by electrical energy.

For a photoanode (photocathode) measured in the three-electrode configuration, the product of the potential gain and the photocurrent could be regarded as the hypothetical half-cell

Published on 13 January 2014. Downloaded by Indian Institute of Technology Chennai on 07/02/2017 06:22:37.

solar-to-hydrogen efficiency (HC-STH). The gain in potential by PEC water splitting could be approximated by the difference of the potential of a photoanode (photocathode) from the oxygen (hydrogen) equilibrium potential:

$$\text{HC-STH} = \begin{cases} \dfrac{|j| \times \left(E_{O_2/H_2O} - E_{RHE}\right)}{P_{sun}} (\text{for photoanodes}) \\ \dfrac{|j| \times \left(E_{RHE} - E_{H^+/H_2}\right)}{P_{sun}} (\text{for photocathodes}) \end{cases}, \quad (5)$$

where E_{O_2/H_2O} and E_{H^+/H_2} stand for the equilibrium potentials of oxygen evolution (+1.23 V *vs.* RHE) and hydrogen evolution (0 V *vs.* RHE), respectively. Provided that η_F of PEC water splitting is unity and that a counter electrode drives the counter reaction without any overpotential, HC-STH is a convenient estimate of maximum AB-STH of a half-cell independent of properties of a counter electrode. In reality, however, the potential of a counter electrode is not equilibrated with the potential of the redox reaction on the counter electrode as mentioned in the previous section. Therefore, HC-STH should not be regarded as AB-STH.

STH can be used as a universal and practical standard of the performance of photocatalysts and photoelectrodes, although it conveys too much information to understand the performance of photocatalyst and photoelectrode materials in water splitting. To understand material performance and perform reliable measurements, it is necessary to understand diagnostic efficiencies. The activities of photocatalysts and photoelectrodes are often reported as gas evolution rates and photocurrents in photocatalytic and PEC water splitting, respectively, measured using various light sources for convenience. However, it is practically impossible to compare the activities measured in different reaction systems because of variations in the power spectra of light sources. Hence, for a discussion of performance on kinetic basis, it is necessary to compare how much photons contribute to the photocatalytic and PEC reactions. The apparent quantum efficiency (AQY) and the incident photon-to-current efficiency (IPCE) can be used as standard measures of activity. The AQY is defined as

$$\text{AQY} = \frac{nR}{I}, \quad (6)$$

where n, R, and I denote the number of electrons involved in the photocatalytic reaction, the production rate of molecules, and the rate of incident photons, respectively. In overall water splitting using a single photocatalyst, the constant n for the hydrogen and oxygen evolution rates is equal to two and four, respectively. IPCE is defined as the ratio of the number of electrons passing through an external circuit as a photocurrent to the number of photons irradiating a photoelectrode. Thus, IPCE corresponds to the external quantum efficiency. If the total absorptance of a photoelectrode is available, the absorbed photon-to-current efficiency (APCE) can be calculated by dividing IPCE by the absorptance. It should be again noted that the photocurrent used for the calculation of IPCE and APCE is not necessarily attributable to the water splitting reaction unless the production of hydrogen and oxygen is confirmed at the faradaic efficiency of unity.

AQY, IPCE, and APCE are dependent on the wavelengths of photons, typically decreasing as the irradiation wavelength approaches the absorption edge wavelength because of the lower absorption coefficients and longer migration distances for photoexcited carriers. Therefore, the above efficiencies are usually determined under monochromated irradiation. Note that in most cases, AQY, IPCE, and APCE depend on the light intensity. A number of previous studies have reported that AQY decreased with increasing light intensity because in the high-intensity region, charge recombination was a second-order reaction with respect to light intensity.[6] If AQY and IPCE spectra are independent of the photon flux, it should be possible to reproduce observed water splitting rates and photocurrents from the power spectrum of a light source and the AQY and IPCE spectra, respectively.

c. Test reaction with sacrificial reagents

Photocatalytic water splitting remains challenging because it is an uphill reaction associated with the rapid recombination of photoexcited electrons and holes. Indeed, the kinds of photocatalysts that are capable of steady overall water splitting under visible light are very limited.[4,8,9] An electron donor such as methanol and an electron acceptor such as the silver cation are often added to the reaction solution to measure the photocatalytic activity for the hydrogen and oxygen reactions, respectively.[9,29] These additives are more reactive than water, consumed irreversibly, and are called sacrificial reagents. For example, the standard electrode potential for reduction of carbonic acid to methanol ($E^0_{H_2CO_3(aq)/CH_3OH}$, +0.04 V) is more negative than that for reduction of oxygen to water ($E^0_{O_2/H_2O}$, +1.23 V). That is, methanol is thermodynamically more easily oxidized than water. Similarly, the standard electrode potential for reduction of proton to hydrogen ($E^0_{H^+/H_2}$, 0 V by definition) is more negative than that for reduction of silver cation to metallic silver ($E^0_{Ag^+/Ag}$, +0.80 V). Therefore, silver cation is more easily reduced than proton from the thermodynamic perspective. Undesirable recombination reactions can be suppressed in the presence of sacrificial reagents because photoexcited electrons and holes can be consumed by the sacrificial reagents irreversibly and rapidly. The overall reactions in the presence of methanol or silver ions can be expressed as follows:

$$CH_3OH + H_2O \rightarrow CO_2 + 3H_2 \quad (7)$$

$$4Ag^+ + 2H_2O \rightarrow O_2 + 4Ag^0 + 4H^+ \quad (8)$$

Clearly, the energy gains by the above reactions are much smaller than that of water splitting. Thus, these reactions are not intended for solar energy conversion. Sacrificial photocatalytic water splitting can proceed as long as the thermodynamic requirement for hydrogen or oxygen evolution is satisfied. The bottom of the conduction band should be more negative than the hydrogen evolution potential when hydrogen is evolved from an aqueous methanol solution under light irradiation.

 This journal is © The Royal Society of Chemistry 2014

Published on 13 January 2014. Downloaded by Indian Institute of Technology Chennai on 07/02/2017 06:22:37.

Likewise, the top of the valence band should be more positive than the oxygen evolution potential when oxygen is evolved from an aqueous silver ion solution. Note that a photocatalyst is not necessarily active for overall water splitting even if it is active for both the sacrificial hydrogen and oxygen evolution reactions, because charge separation is strongly supported by sacrificial reagents. Moreover, the determinants of the photocatalytic activity for sacrificial hydrogen and oxygen evolution are not necessarily identical.[29] However, this does not present a problem for the estimation of the charge separation efficiency of photoelectrodes, where either reduction or oxidation reaction proceeds on the surface.[30,31] Given that sacrificial reagents consume all the photoexcited carriers reaching the surface, a photocurrent observed in the presence of sacrificial reagents reflects the flux of minority carriers that have escaped recombination with majority carriers. If the absorptance of a photoelectrode is available, one can estimate the efficiencies of charge separation inside the photoelectrode and charge injection on the surface.[30]

5. Advancements in photocatalytic water splitting

a. Overall water splitting using a single photocatalyst

Some transition metal oxides with d^0 electronic configuration and typical metal oxides with d^{10} electronic configuration show activity for photocatalytic water splitting under UV light illumination. In particular, $NaTaO_3$ doped with La[32] and Ga_2O_3 doped with Zn[33] exhibit the highest water splitting rates when modified with NiO and $Rh_{2-y}Cr_yO_3$ cocatalysts, respectively. Cocatalyst loading is, in fact, essential to achieve efficient photocatalytic water splitting. The function of NiO and $Rh_{2-y}Cr_yO_3$ for various photocatalysts has been attributed to the facilitation of hydrogen evolution processes by various methods, including the sacrificial water splitting reaction[27,32] and transient absorption spectroscopy[34] with and without cocatalyst loading. In the absence of cocatalysts, oxide photocatalysts exhibit decent activity for the sacrificial oxygen evolution reaction but not for the sacrificial hydrogen evolution reaction. These results indicate that the surface of oxide photocatalysts is hardly active for hydrogen evolution. Loading of NiO and $Rh_{2-y}Cr_yO_3$ significantly improves the hydrogen evolution activity and thus enables overall water splitting. In addition, photoexcited electrons in the conduction band were found to be quenched by the loading hydrogen evolution cocatalyst, indicating that electrons were trapped by the cocatalyst and thus separated from photoexcited holes. Therefore, cocatalysts can facilitate both charge separation and surface kinetics. It is preferable for an ohmic contact to be formed between the photocatalyst and hydrogen evolution cocatalyst so that electrons can be injected into the cocatalyst preferentially. Otherwise, a cocatalyst would also function as a recombination centre. It was demonstrated by spectroscopy under potential control that a Schottky-type barrier was present at the interface between an n-type GaN single crystal and Pt particles.[35] Thus, electron migration from GaN to Pt is suppressed while holes can be injected without an energy barrier.

The kinds of non-oxide photocatalysts that are active for overall water splitting are limited because of the weaker reactivity of the photoexcited carriers owing to the smaller band gap energies and the difficulties in preparing materials with adequate quality. However, certain non-oxide photocatalysts become active for overall water splitting through appropriate modification with hydrogen evolution cocatalysts. As for metal oxynitrides, solid solutions of GaN and ZnO ($(Ga_{1-x}Zn_x)(N_{1-x}O_x)$) and $ZnGeN_2$ and ZnO ($(Zn_{1+x}Ge)(N_2O_x)$), for example, are capable of overall water splitting after loading of hydrogen evolution cocatalysts.[9] In particular, $(Ga_{1-x}Zn_x)(N_{1-x}O_x)$ modified with $Rh_{2-y}Cr_yO_3$ holds the highest AQY for overall water splitting using a single photocatalyst under visible light (5.1% at 410 nm).[2] Recently, ZrO_2-modified TaON (ZrO_2/TaON), a transition metal oxynitride, was also reported to be active for overall water splitting when coloaded with cocatalysts for both hydrogen and oxygen evolution.[36]

Loading of oxygen evolution cocatalysts has a weaker effect on the photocatalytic activity than loading of hydrogen evolution cocatalysts. Loading of Mn_3O_4 alone as an oxygen evolution cocatalyst on $(Ga_{1-x}Zn_x)(N_{1-x}O_x)$ does not enable overall water splitting because of the lack of hydrogen evolution sites.[37] Loading of Mn_3O_4, RuO_2, and IrO_2 as oxygen evolution cocatalysts is effective when they are coloaded on the photocatalyst together with a hydrogen evolution cocatalyst such as Rh/Cr_2O_3 core/shell composite.[37,38] However, the optimal loading amounts of oxygen evolution cocatalysts were below 0.05 wt% (see Fig. 4), whereas the typical loading amount of $Rh_{2-y}Cr_yO_3$ as a hydrogen evolution cocatalyst was 1 wt% (for Rh alone) or larger.[38] In addition, coloading of oxygen evolution cocatalysts improved the water splitting rates by a factor of 1.4 at most, regardless of the kinds of cocatalysts. These results suggest that photocatalytic activity was limited by the hydrogen evolution process.

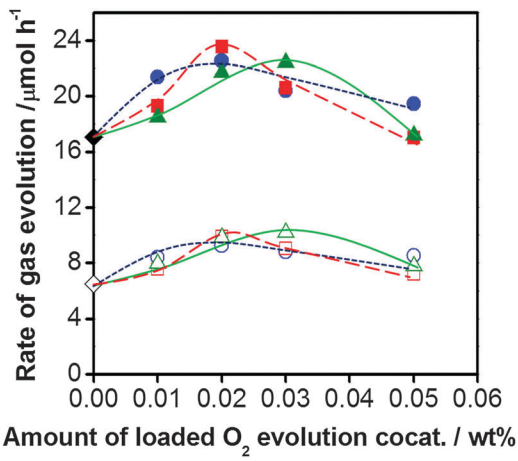

Fig. 4 The photocatalytic activity of GaN:ZnO coloaded with different O_2 evolution cocatalysts and Rh/Cr_2O_3 for water splitting under visible light ($\lambda > 420$ nm). Circles, triangles, and squares indicate the loading of Mn_3O_4, IrO_2, and RuO_2, respectively. Closed and open symbols denote H_2 and O_2, respectively.[38] ©2013 Wiley-VCH Verlag GmbH & Co. KGaA, Weinheim.

Published on 13 January 2014. Downloaded by Indian Institute of Technology Chennai on 07/02/2017 06:22:37.

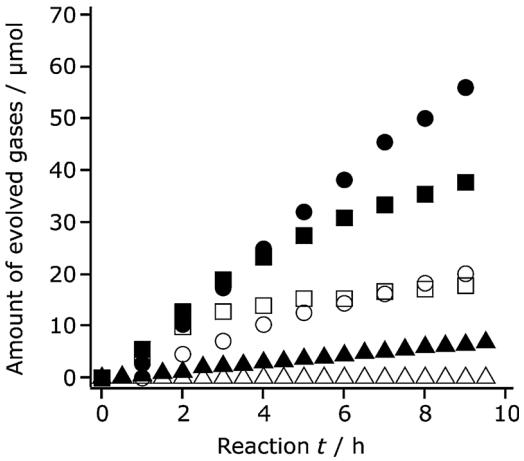

Fig. 5 Time courses of water splitting under UV irradiation (λ > 300 nm) using ZrO_2/TaON after various modifications (● = H_2 ($IrO_2/Cr_2O_3/RuO_x$), ○ = O_2 ($IrO_2/Cr_2O_3/RuO_x$), ■ = H_2 (Cr_2O_3/RuO_x), □ = O_2 (Cr_2O_3/RuO_x), ▲ = H_2 (RuO_x), △ = O_2 (RuO_x)).[36] ©2013 WILEY-VCH Verlag GmbH & Co. KGaA, Weinheim.

Although the catalytic enhancement was not dramatic, coloading of oxygen evolution cocatalysts did improve the durability of non-oxide photocatalysts significantly because photooxidation of water and of the photocatalyst itself competed on the surface. It was reported that coloading of RuO_2 on $(Ga_{1-x}Zn_x)(N_{1-x}O_x)$ together with Rh/Cr_2O_3 suppressed the loss of nitrogen on the photocatalyst during photocatalytic water splitting.[39] As a result, deactivation of the photocatalyst was also suppressed. ZrO_2/TaON modified with the RuO_x/Cr_2O_3 core/shell composite as a hydrogen evolution cocatalyst showed activity for overall water splitting, although the gas evolution rates decreased with time because of the deactivation of the photocatalyst (Fig. 5).[36] When IrO_2 was coloaded as an oxygen evolution cocatalyst on ZrO_2/TaON with RuO_x/Cr_2O_3, overall water splitting proceeded steadily. This result stresses the importance of stabilizing non-oxide photocatalysts against water oxidation by modification with oxygen evolution cocatalysts for long operations.

b. Z-scheme water splitting

Overall water splitting has been achieved with some single non-oxide photocatalysts, as mentioned in the previous section. However, the absorption edge wavelengths of the active photocatalysts were 500 nm at most, which was too short to harvest sunlight effectively. Z-scheme water splitting is advantageous over one-step photoexcitation water splitting in that a wider range of visible light can be used, as semiconductors with either water reduction or oxidation potentials can be employed. In fact, WO_3[40] and $BiVO_4$[16,18] are applied as oxygen evolution photocatalysts in Z-scheme water splitting. Furthermore, $BaTaO_2N$, whose absorption edge wavelength is 660 nm, is applicable as a hydrogen evolution photocatalyst.[41] On the other hand, the number of photons required to generate a given amount of hydrogen is double that required for one-step splitting. In addition, the Z-scheme requires balanced photocatalytic activity of the hydrogen and oxygen evolution photocatalysts under shared pH conditions and redox mediator concentrations.

In Z-scheme water splitting, it is critical to suppress backward reactions involving redox mediators that are thermodynamically more favourable than water splitting. To avoid side reactions, forward reactions should proceed efficiently. The highest AQY of 6.3% at 420 nm was achieved with a Z-scheme system based on Pt-loaded ZrO_2/TaON as a hydrogen evolution photocatalyst, Pt-loaded WO_3 as an oxygen evolution photocatalyst, and IO_3^-/I^- as a redox couple (Fig. 6).[40] I^- ions as a donor and IO_3^- ions as an acceptor react efficiently on Pt-loaded ZrO_2/TaON and Pt-loaded WO_3, respectively. As a result, undesirable backward reactions such as oxidation of I^- ions on Pt-loaded WO_3 and reduction of IO_3^- on Pt-loaded ZrO_2/TaON are minimized. Modifying TaON with ZrO_2 was essential to render TaON active for hydrogen evolution.

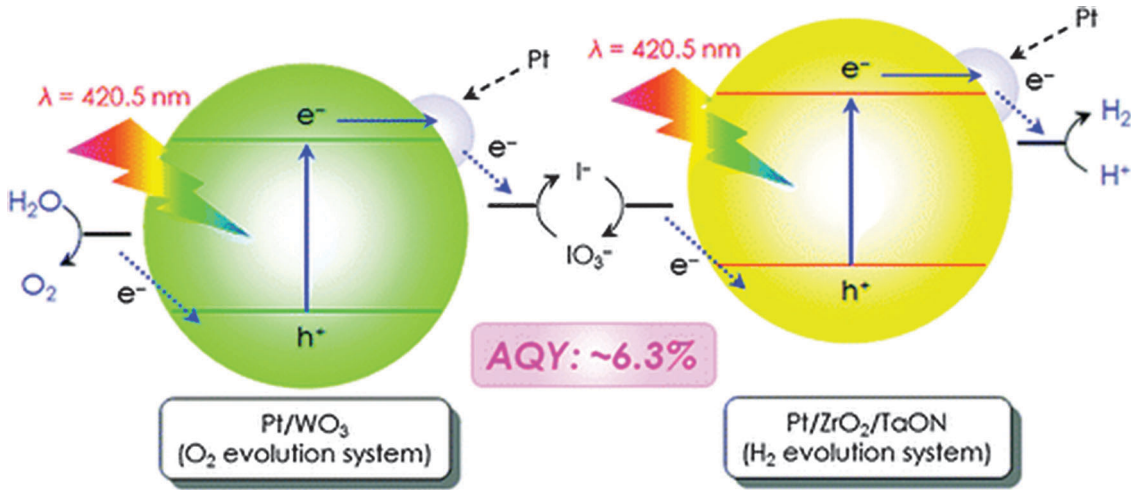

Fig. 6 Schematic reaction mechanism of Z-scheme water splitting using Pt/ZrO_2/TaON, Pt/WO_3, and IO_3^-/I^- as the hydrogen evolution photocatalyst, oxygen evolution photocatalyst, and reversible redox mediator, respectively. Reprinted with permission from ref. 40. ©2010 American Chemical Society.

Published on 13 January 2014. Downloaded by Indian Institute of Technology Chennai on 07/02/2017 06:22:37.

Table 1 Effect of the weight ratio of Pt/ZrO_2/TaON–Pt/WO_3–NaI in the reaction solution on water splitting activity under monochromatic light irradiation (λ > 420.5 nm)[40]

Pt/ZrO_2/TaON–Pt/WO_3–NaI (mg)	Concn of NaI (mM)	Loading amt of Pt on ZrO_2/TaON (wt%)	Gas evolution rate (μmol h^{-1})		
			H_2	O_2	AQY (%)
50–100–15	1.0	1.0	3.3	1.6	2.7
25–50–7.5	0.5	1.0	5.5	2.7	4.3
10–20–3.0	0.2	1.0	4.6	2.1	3.5
10–20–15	1.0	1.0	4.3	1.4	2.3
25–50–7.5	0.5	0.5	7.5	3.8	6.3
25–50–7.5	0.5	0.1	<1		n.d.

Adapted with permission from ref. 40. ©2010 American Chemical Society.

Photoluminescence spectroscopy and PEC measurements revealed that the n-type semiconducting character of TaON was moderated as a result of the ZrO_2 modification. This would extend the lifetime of photoexcited holes in ZrO_2/TaON owing to the lower density of the inherent electrons. In addition, reaction conditions such as Pt loading and concentrations of photocatalysts and of redox mediators should be optimized so that photoexcited electrons are consumed in hydrogen evolution instead of the reduction of IO_3^- ions, as shown in Table 1.[40]

The combination of Ru-loaded $SrTiO_3$ doped with Rh ($SrTiO_3$:Rh) for hydrogen evolution and $BiVO_4$ for oxygen evolution works efficiently in Z-scheme water splitting in the presence of various reversible redox couples. In particular, the use of $[Co(bpy)_3]^{3+/2+}$ as a redox couple exhibited excellent AQY (2.1% at 420 nm) for overall water splitting although this redox couple was not effective for other combinations of photocatalysts.[41] This Z-scheme system works stably and shows decent hydrogen and oxygen evolution under natural sunlight. It is also possible to generate hydrogen and oxygen separately by dispersing the hydrogen evolution photocatalyst and the oxygen evolution photocatalyst in a two-chamber cell separated by a membrane filter penetrating the redox couple. The choice of the reaction pH plays a key role in maximizing the reaction efficiency of the Z-scheme system. This is because the potentials of the band edges of the oxide photocatalysts depend on the pH of the reaction solution, while the redox potential of $[Co(bpy)_3]^{3+/2+}$ does not. Accordingly, the potential of the redox couple relative to the band edges is also dependent on pH. As shown in Fig. 7, with decreasing pH, the potential of $[Co(bpy)_3]^{3+/2+}$ shifts to more negative potentials against the band edges of $SrTiO_3$:Rh and $BiVO_4$.[41] As a result, the oxidation of $Co(bpy)^{2+}$ for hydrogen evolution on Ru-loaded $SrTiO_3$:Rh was enhanced. However, the reduction of $Co(bpy)^{3+}$ on $BiVO_4$ for oxygen evolution became difficult owing to the smaller energy offset between the conduction band edge of $BiVO_4$ and the reduction potential of $Co(bpy)^{3+}$. Furthermore, oxidation of $Co(bpy)^{2+}$ occurred significantly on $BiVO_4$. As a result, the activity for Z-scheme water splitting decreased dramatically with decreasing pH. In contrast, the reduction of $Co(bpy)^{3+}$ for oxygen evolution on $BiVO_4$ was facilitated, while the oxidation of $Co(bpy)^{2+}$ for hydrogen evolution on Ru-loaded $SrTiO_3$:Rh was suppressed at higher pH values. Consequently, the highest activity was observed at neutral pH.

Interestingly, it was found that a mixture of Ru-loaded $SrTiO_3$:Rh and $BiVO_4$ generated hydrogen and oxygen stoichiometrically even in the absence of redox mediators.[16] The activity for overall water splitting was highly dependent on the pH of the reaction solution, peaking steeply at pH 3.5. Optical microscopy of suspensions of Ru-loaded $SrTiO_3$:Rh and $BiVO_4$ revealed that particles of both photocatalysts aggregated best at pH 3.5, while they hardly aggregated at pH 7. This was due to the sign of the electrostatic charge of the photocatalyst particles. The isoelectric point of Ru-loaded $SrTiO_3$:Rh was approximately 4, meaning that the powder is negatively charged at pH > 4 and positively charged at 2 < pH < 4. On the other hand, $BiVO_4$ was negatively charged even at pH 2. Therefore, Ru-loaded $SrTiO_3$:Rh and $BiVO_4$ had an electrostatic attractive force in an aqueous solution at pH < 4, forming aggregates composed of both photocatalysts. It was confirmed that the photoluminescence of $BiVO_4$ was quenched by mixing active $SrTiO_3$:Rh containing surface Rh species whose oxidation state was reversible, which was indicative of electron transfer from $BiVO_4$ to $SrTiO_3$:Rh *via* physical contact. Additionally, water

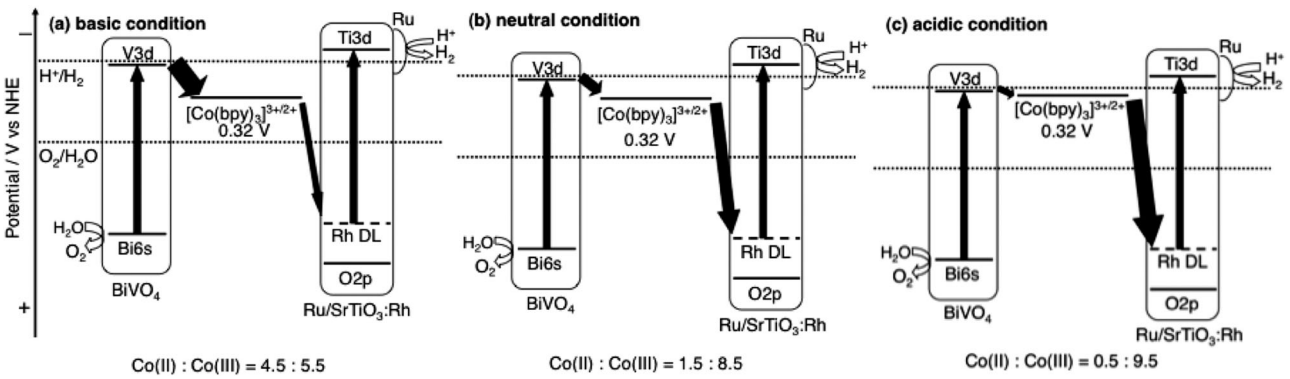

Fig. 7 Energy diagrams of the Z-scheme photocatalyst system, (Ru/$SrTiO_3$:Rh)–($BiVO_4$)–($[Co(bpy)_3]^{3+/2+}$), and the ratio of $[Co(bpy)_3]^{2+}$ ions to $[Co(bpy)_3]^{3+}$ ions during overall water splitting under basic, neutral, and acidic conditions. Reprinted with permission from ref. 41. ©2013 American Chemical Society.

Published on 13 January 2014. Downloaded by Indian Institute of Technology Chennai on 07/02/2017 06:22:37.

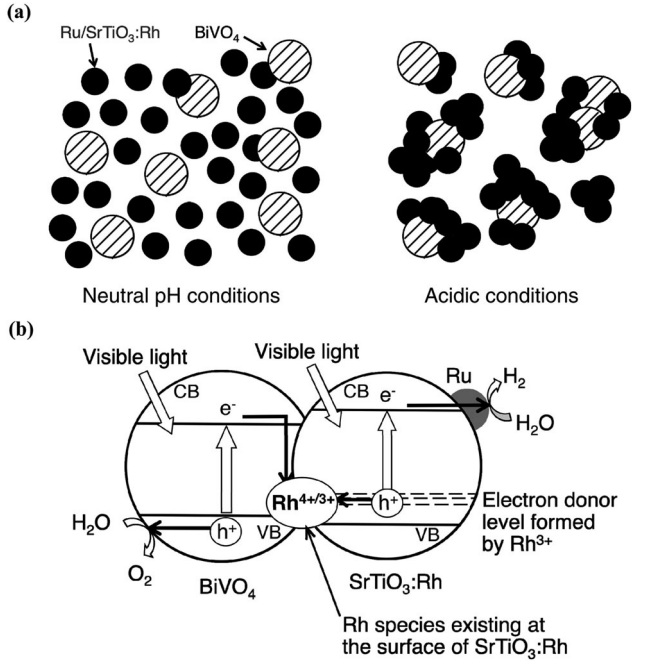

Fig. 8 Mechanism of water splitting using the Z-scheme photocatalysis system driven by electron transfer between H_2- and O_2-photocatalysts. (a) Suspension of Ru/$SrTiO_3$:Rh and $BiVO_4$ under neutral and acidic conditions. (b) Scheme of photocatalytic water splitting. Reprinted with permission from ref. 16. ©2009 American Chemical Society.

splitting did not proceed when the two photocatalysts were physically separated, further stressing the importance of the interaction of the two photocatalysts. The above results indicate that Z-scheme water splitting took place *via* interparticle electron transfer and thus physical contact between the two photocatalysts was necessary to complete the process (Fig. 8).[16]

Z-scheme water splitting *via* interparticle electron transfer can be advantageous over conventional Z-scheme water splitting with reversible redox couples in that thermodynamically favourable backward reactions involving reversible redox couples do not occur. Therefore, (oxy)nitride photocatalysts that have a low selectivity for the forward reaction, such as Ta_3N_5, can be applied to Z-scheme water splitting without elaborate surface modification. For example, a suspension of Ru-loaded $SrTiO_3$:Rh and Ir/CoO_x-coloaded Ta_3N_5 shows activity for Z-scheme water splitting and potentially utilizes photons up to 600 nm for oxygen evolution on Ta_3N_5.[17] The activity was significantly dependent on the pH of the reaction solution, peaking at pH 3.9. Unlike $BiVO_4$, the use of Ta_3N_5 did not lead to steady water splitting although Ta_3N_5 is active for oxygen evolution as long as photoexcited electrons are scavenged. A major challenge in this Z-scheme water splitting system was facilitating interparticle electron transfer between $SrTiO_3$:Rh and Ta_3N_5. It was found that Ir loaded on Ta_3N_5 effectively captured the photoexcited electrons of Ta_3N_5, facilitated the electron transfer to $SrTiO_3$:Rh *via* physical contact, and was thus necessary to achieve Z-scheme water splitting. In addition, coloading of CoO_x as an oxygen evolution cocatalyst was found to improve the durability of the Z-scheme system, similarly to overall water splitting on $(Ga_{1-x}Zn_x)(N_{1-x}O_x)$.[39]

c. Sacrificial water oxidation

Although oxygen evolution rates in the presence of Ag^+ cations would not necessarily be relevant to the activity for overall water splitting,[29] photocatalyst–cocatalyst composites efficient for the sacrificial oxygen evolution are expected to be applicable as photoanodes in PEC water splitting, because loading oxygen evolution cocatalysts can improve charge separation efficiency greatly. In addition, development of oxygen evolution cocatalysts for non-oxide photocatalysts contributes to stabilization of the materials against self-oxidation. Nanoparticles of Mn_3O_4, RuO_2, and IrO_2 were found to function as oxygen evolution cocatalysts, as mentioned previously.[38] In addition, cobalt oxide has received much attention as an efficient cocatalyst for oxygen evolution on non-oxide photocatalysts. Cobalt oxide nanoparticles can be loaded on $LaTiO_2N$ by impregnation with an aqueous solution of Co salts followed by nitridation treatment typically at 973 K.[42] The Co species after nitridation is often a mixture of divalent and trivalent oxides and will be denoted as CoO_x hereafter for simplicity. $LaTiO_2N$ modified with CoO_x exhibited higher photocatalytic activity for the oxygen evolution reaction from an aqueous silver nitrate solution than did $LaTiO_2N$ modified with IrO_2, a conventional oxygen evolution cocatalyst. In particular, AQY reached 27% at 440 nm for the oxygen evolution reaction when single-crystalline mesoporous and macroporous $LaTiO_2N$ was used as a photocatalyst.[42] This efficiency is significantly higher than those reported for photocatalysts with a 600 nm absorption edge. The activity enhancement is believed to be associated with improvements in both the photocatalyst and cocatalyst components. The single-crystalline $LaTiO_2N$ with its porous interior not only provided more active surface area but also lowered the defect density, which would have suppressed the recombination of photogenerated carriers. In addition, time-resolved infrared absorption spectroscopy revealed that the deposition of either CoO_x or IrO_2 enhanced the lifetime of excited electrons with respect to unmodified LTON (Fig. 9).[42] In particular, the

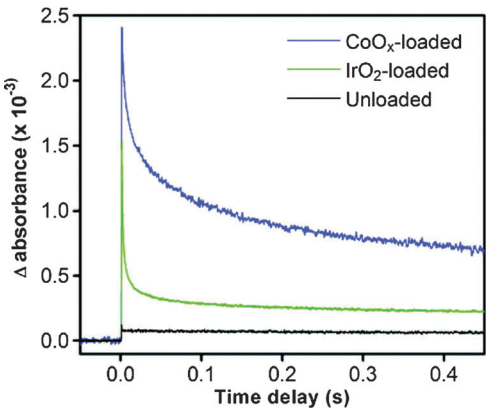

Fig. 9 Decay of photogenerated electrons on $LaTiO_2N$ prepared *via* the flux method with and without cocatalysts: (a) $LaTiO_2N$; (b) IrO_2/$LaTiO_2N$; and (c) CoO_x/$LaTiO_2N$. The catalysts were irradiated by a 355 nm UV pulse at 1 mJ, and the transient absorption was observed at 2000 cm^{-1}. Reprinted with permission from ref. 42. ©2012 American Chemical Society.

 This journal is © The Royal Society of Chemistry 2014

Published on 13 January 2014. Downloaded by Indian Institute of Technology Chennai on 07/02/2017 06:22:37.

lifetime of carriers was prolonged more by the deposited CoO_x, to a time scale of seconds. This indicates that both CoO_x and IrO_2 play a role in separating the photogenerated electrons and holes, and the better separation of carriers with CoO_x modification explains the higher photocatalytic performance observed with CoO_x modification compared to IrO_2 modification.

CoO_x was also effective for nitride and oxysulphide photocatalysts such as Ta_3N_5[17,43] and $Sm_2Ti_2S_2O_5$.[44] Modification of Ta_3N_5 with nanoparticulate CoO_x enhanced the activity for water oxidation activity and suppressed nitrogen evolution because of decomposition of the nitride.[17,43] Besides, the surface modification of Ta_2O_5 with alkaline metal salts was found to improve the water oxidation activity of Ta_3N_5.[43] Ta_3N_5 nitrided from Ta_2O_5 modified with Na_2CO_3 exhibited better crystallinity, smaller particles with smoother surfaces, and a six-fold improvement in photocatalytic activity for oxygen evolution under visible light. It is believed that the partial dissolution of Ta_2O_5 with Na_2CO_3 and nucleation of $NaTaO_3$ grains in the early stage of the nitridation gave rise to the characteristic particle morphologies and improved activity. Loading of CoO_x onto the modified Ta_3N_5 as an oxygen evolution cocatalyst by nitridation treatment at 773 K further improved the photocatalytic activity, yielding an AQY of 5.2% at 500–600 nm.[43]

CoO_x-loaded $Sm_2Ti_2S_2O_5$ was prepared by sulphurization of SmTi oxide impregnated with an aqueous solution of $Co(NO_3)_2$ at 1223 K under a H_2S flow followed by calcination in air.[44] During the sulphurization, Co species decomposed into Co_3O_4 and then CoS_x (mixture of Co_3S_4 and CoS) and finally oxidized into CoO_x. The AQY was estimated to be 5% at 420 nm, the highest among oxysulphides ever reported. Accordingly, CoO_x loaded by nitridation and sulphurization treatments worked as an efficient oxygen evolution cocatalyst for (oxy)nitrides and oxysulphides. The treatment temperatures were 773 K or higher. This is considerably higher than the temperatures applied to deposit nanoparticles of noble metals or metal oxides as cocatalysts,[27,32,33] which might allow for a more intimate interaction between the photocatalyst and cocatalyst.

6. Advancements in photoelectrochemical water splitting

a. Preparation of electrodes

Photoelectrodes of non-oxide semiconductors can be fabricated using powdered materials synthesized in advance.[45,46] They can also be synthesized directly on conductive substrates by nitridation/sulphurization of metals and metal oxides[20,22] and by vacuum processes such as molecular beam epitaxy (MBE),[19] radio-frequency (RF) magnetron sputtering, chemical vapour deposition (CVD), and vacuum evaporation. Generally, it is important to establish good electric contact between semiconductor particles/layers and a conductive substrate and reduce density of grain boundaries across the photoelectrode in order to minimize series resistance.

Drop casting, squeegeeing, and electrophoretic deposition can be used to coat conductive substrates with powdered semiconductor materials. However, the PEC performance as well as mechanical strength of such photoelectrodes is generally poor because of the high resistance between particles and substrates. To facilitate charge transfer between semiconducting particles and a conductive substrate, necking treatments are usually applied.[46] Photoelectrodes made of powdered semiconductors are treated with solvents containing appropriate metal salt precursors. Subsequently, the modified photoelectrodes are annealed under appropriate conditions, *e.g.*, under an NH_3 flow in the case of (oxy)nitride photoelectrodes. During the heating, the metal salts decompose into metal oxide and/or (oxy)nitride and bridge the semiconducting particles. One of the problems of the necking treatment is the durability of semiconductor particles and conductive substrates during the heat treatment. For example, (oxy)nitrides layers modified with metal salts should be heated under an NH_3 flow at high temperatures to ensure intimate contact between particles and necking agents and to suppress decomposition. However, transparent conductive oxides such as fluorine-doped SnO_2 and tin-doped In_2O_3 cannot be handled at high temperatures especially under an NH_3 atmosphere.

Recently, the particle transfer method was developed as an alternative to necking treatment.[45] The particle transfer process is illustrated in Fig. 10. First, a semiconducting powder is laid on a glass substrate. Then, a thin metal layer (approximately 100–300 nm) is deposited as a contact layer by the sputtering method. The choice of metal is considered to be key to establishing a favourable electrical contact between the semiconductor particles and the metal layer. After that, continuous metal films several micrometers in thickness are deposited by the sputtering method for adequate conductivity and mechanical strength. The resulting metal film is transferred to another substrate by a resin, and the primary substrate is peeled off. The excess powder is removed by ultrasonication in water. This method ensures an adequate electrical contact between the semiconducting particles and metal layer. In addition, since

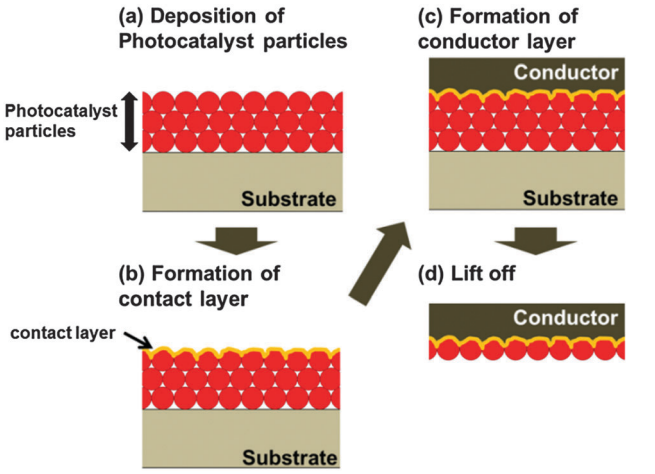

Fig. 10 Schematic of the particle transfer method. Reproduced from ref. 45 with permission from The Royal Society of Chemistry. © Royal Society of Chemistry 2013.

Published on 13 January 2014. Downloaded by Indian Institute of Technology Chennai on 07/02/2017 06:22:37.

the semiconductor particles attached loosely to the electrodes are removed, a mono-particle layer covers the metal conductor film. It should be noted that the process is applicable to a variety of powdered semiconductors in the fabrication of photoelectrodes.

The application of nanorods grown vertically on conductive substrates is advantageous over other types of photoelectrodes because the photogenerated minority carriers arrive at the electrolyte interface sooner in the case of submicron-diameter nanorods. The majority carriers are transferred easily within the core of nanorods along their long axis. Among the various non-oxide materials, one-dimensional Ta_3N_5 nanorod arrays have been identified as a promising candidate for solar-driven PEC water splitting.[47] Vertically aligned Ta_3N_5 nanorod arrays can be fabricated by nitridation of Ta_2O_5 nanorod arrays grown *via* a through-mask anodization method. First, a porous anodic alumina (PAA) mask was formed on top of a Ta substrate by anodizing an evaporated Al layer. Ta_2O_5 nanorods were then embedded into the nanochannels of the PAA mask by anodizing the Ta substrate through the PAA mask in an aqueous solution of boric acid (0.5 M). Owing to the low solubility of Ta^{5+} in the boric acid solution and the volume expansion associated with the anodization of Ta into Ta_2O_5, the Ta_2O_5 filled into the nanochannels of the PAA mask under a high electrical field. Subsequently, the PAA mask was selectively etched with 5% phosphoric acid, yielding Ta_2O_5 nanorod arrays. Finally, the Ta_2O_5 nanorod arrays were nitrided into Ta_3N_5 nanorod arrays under a heated NH_3 flow. The whole fabrication process and the SEM images of typical Ta_3N_5 nanorod arrays are shown in Fig. 11.

b. Photoanodes

Photoanodes consisting of n-type semiconductors evolve oxygen at the interfaces between the photoanodes and electrolytes. The photoexcited holes generated in an n-type semiconductor migrate to the interface and oxidize water to oxygen. Therefore, the surface of the photoanode is likely to be oxidized. Appropriate surface modifications catalysing the oxygen evolution reaction are thus required to obtain a high photocurrent and stability.

Fig. 12 shows the current–potential curves of $LaTiO_2N$ photoanodes in a 1 M aqueous Na_2SO_4 solution at pH = 13.5.[45] This photoelectrode was prepared by the particle transfer method using Ta and Ti layers as the contact layer and

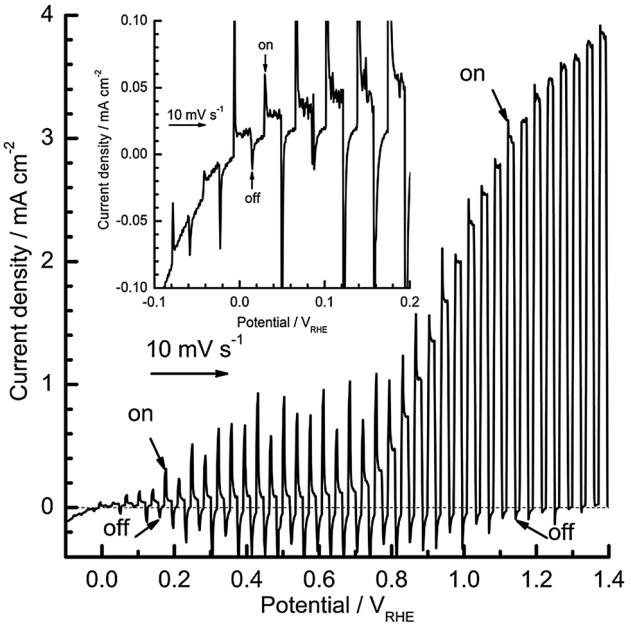

Fig. 12 Current–potential curve of IrO_2-loaded $LaTiO_2N$ electrodes with a Ta contact layer between the $LaTiO_2N$ particles and the Ti conductor layer: the electrolyte was a 1 M aqueous Na_2SO_4 solution with pH = 13.5, adjusted by the addition of NaOH. Simulated sunlight (AM1.5D) was turned on and off with a periodicity of 6 s. The electrode potential was swept in the positive direction at a rate of 10 mV s^{-1}. Reproduced from ref. 45 with permission from The Royal Society of Chemistry. © Royal Society of Chemistry 2013.

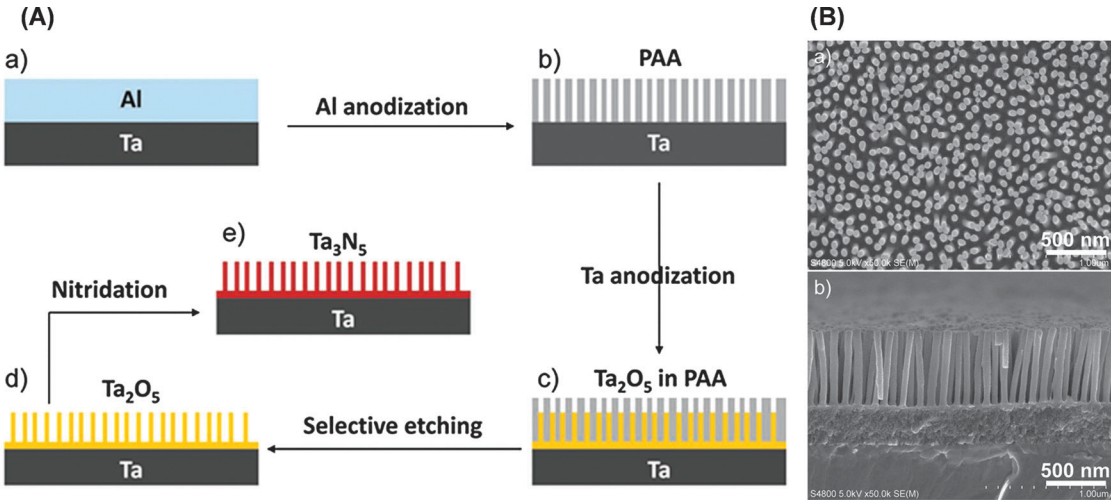

Fig. 11 (A) Schematic of the fabrication process and (B) SEM images of an array of vertically aligned Ta_3N_5 nanorods.[47] ©2013 WILEY-VCH Verlag GmbH & Co. KGaA, Weinheim.

Published on 13 January 2014. Downloaded by Indian Institute of Technology Chennai on 07/02/2017 06:22:37.

conductor layer, respectively.[45] The surface of the photoanode was modified with IrO_2 as an oxygen evolution catalyst. The anodic photocurrent was observed below 0 V *vs.* RHE. This indicates that the potential of the conduction band minimum of $LaTiO_2N$ was more negative than the equilibrium potential of hydrogen evolution. The appearance of a photocurrent below 0 V *vs.* RHE suggests that $LaTiO_2N$ has a band structure appropriate for unassisted overall water splitting. When a PEC system splits water by the energy of light alone, the potential of the photoanode must be more negative than 0 V *vs.* RHE so that a counter electrode can evolve hydrogen.

IrO_2 is one of the most active oxygen evolution catalysts. However, the amount of Ir available on Earth is critically limited. The Co species with phosphate (CoPi) has attracted much attention as an oxygen-evolving catalyst.[48] In foresight of large-scale applications, the development of oxygen evolution cocatalysts consisting of earth-abundant elements such as CoPi is important.

c. Photocathodes

Photocathodes consist of p-type semiconductors and evolve hydrogen at the interface between semiconductor particles and electrolytes. In the case of photocathodes, a reduction reaction takes place, so that the possibility of oxidative degradation is lower than that for photoanodes. However, the number of inherent p-type semiconductors is relatively small. Most oxide, nitride, and sulphide semiconductors are n-type, likely because of anion defects. Certain Cu-based chalcogenides exhibit p-type conductivity and a promising performance in photovoltaic applications.

Fig. 13 shows the current–potential curves of $CuGaSe_2$ photoelectrodes prepared by MBE on a Mo-coated glass substrate.[26] The photoelectrode surface was modified with Pt to catalyse the hydrogen evolution reaction. A cathodic photocurrent due to hydrogen evolution was observed below *ca.* 0.7 V *vs.* RHE. With the deposition of 40 nm-thick CdS on $CuGaSe_2$, the cathodic photocurrent was markedly enhanced. CdS is an n-type semiconductor and can form a good p–n heterojunction with $CuGaSe_2$. The band-bending initiated in CdS on $CuGaSe_2$ is the key to enhancing the photocurrent. An analogous attempt has been made for an n-type photoelectrode. $CaFe_2O_4$ is a unique p-type semiconductor. When an n-type TaON photoelectrode was coated with $CaFe_2O_4$, the photocurrent due to oxygen evolution was enhanced.[49] Such utilization of p–n heterojunctions is effective in improving the onset potential of the photocurrent.

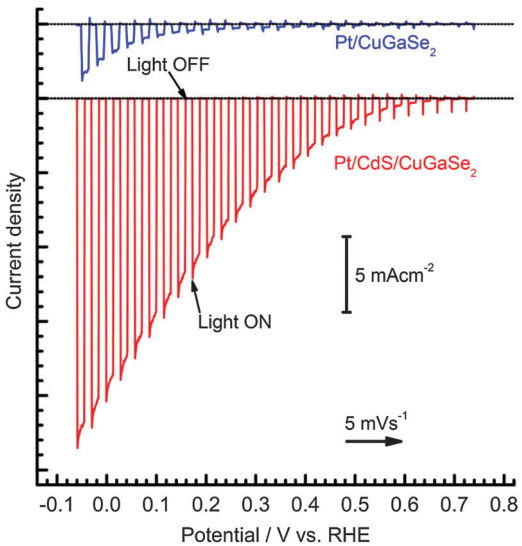

Fig. 13 Current–potential curves for $Pt/CuGaSe_2$ and $Pt/CdS/CuGaSe_2$ electrodes. 0.1 M Na_2SO_4 aq. (pH 9), 300 W Xe lamp, 5 mV s^{-1}. Reprinted with permission from ref. 26. ©2013 American Chemical Society.

H_2 evolution catalysts on photocathodes are usually Pt because of the high catalytic activity, *i.e.*, the high exchange current for the hydrogen evolution reaction. However, Pt is a precious metal and should be replaced by an abundant material. MoS_2 doped with transition metals is one candidate for an alternative H_2 evolution catalyst.[50]

It is difficult to obtain a photocathodic current at the equilibrium potential of oxygen evolution (1.23 V *vs.* RHE) using p-type photoelectrodes, as the valence band maximum of most currently available p-type semiconductors is more negative than that potential. Consequently, they cannot split water in a single step since the potential of the counter electrode is not positive enough to evolve oxygen from water. To split water only by the energy of light using p-type photoelectrodes, a combination with n-type photoelectrodes and/or photovoltaic cells is required. The two-step system can split water without electrical power if the photocurrents of the photoanode and photocathode are balanced at a certain potential.

7. Conclusion

This tutorial review presented the fundamental aspects of photocatalytic and PEC water splitting for conversion of solar energy into hydrogen. To achieve unassisted water splitting using a single semiconductor material, the band gap of the semiconductor must straddle the reduction and oxidation potentials of water so that photoexcited electrons and holes have sufficient overpotential for the hydrogen and oxygen evolution reactions, respectively. Non-oxide materials such as (oxy)nitrides, oxysulphides, and chalgogenides are potential candidates for solar water splitting because the valence band edge is shifted negatively and thus they overcome the problem of large overvoltage loss of oxygen evolution on oxide semiconductors. Z-scheme and tandem systems based on multi-step photoexcitation liberate the semiconducting materials from thermodynamic limitations and enable the application of a variety of materials to unassisted water splitting. However, the suppression of backward reactions and matching of activity for hydrogen evolution and oxygen evolution under operating conditions are important. Fine-tuning of reaction conditions and construction of redox-free Z-scheme systems are possible solutions. In practice, surface modifications are essential in facilitating the charge separation and the surface reaction

Published on 13 January 2014. Downloaded by Indian Institute of Technology Chennai on 07/02/2017 06:22:37.

kinetics, which also improve the durability of photocatalytic and PEC systems for water splitting. The photocatalytic activity of non-oxide materials is likely limited by the hydrogen evolution process considering the kinetic enhancements by hydrogen evolution cocatalysts and oxygen evolution cocatalysts. Nevertheless, the development of oxygen evolution photocatalysts is important for non-oxide materials, particularly for water oxidation, because non-oxides are thermodynamically less stable than oxides in systems involving oxygen and/or water. The reactivity of photoexcited holes should be controlled kinetically. Having fewer grain boundaries and shorter migration distances for photoexcited carriers is important for deriving the potential of semiconductors in PEC water splitting. The particle transfer method and vertically aligned nanorods are promising options. Additionally, the development of p–n junctions assists charge separation in PEC water splitting.

The target of solar energy conversion efficiency by photocatalytic and photoelectrochemical water splitting was set at 10%.[2] Photocatalysts and photoelectrodes should be active for water splitting under irradiation up to 600 nm or even longer to achieve a sufficient solar energy conversion efficiency at a reasonable quantum efficiency. In the long term, the development of semiconductors active even under red and near-infrared rays will become important. Researchers working on semiconductor materials and catalysts for water splitting are responsible for achieving adequate performance in solar-to-hydrogen conversion, because there are also many challenges in separation, purification, transportation, and utilization of solar hydrogen fuel as well as in scale-up. All the above-mentioned research fields are essential to establish a sustainable society based on solar hydrogen.

Acknowledgements

This work was financially supported by Grant-in-Aids for Specially Promoted Research (No. 23000009) and for Young Scientists (B) (No. 25810112) of the Japan Society for the Promotion of Science (JSPS). This work was also supported by JSPS through the Funding Program for World-Leading Innovative R&D on Science and Technology (FIRST), initiated by the Council for Science and Technology Policy (CSTP). Further financial support came from the International Exchange Program of the A3 Foresight Program of JSPS.

References

1 *BP Statistical Review of World Energy June 2013*, BP Statistical Review of World Energy, BP p.l.c, 1 St James's Square, London, SW1Y 4PD, UK.
2 K. Maeda and K. Domen, *J. Phys. Chem. Lett.*, 2010, **1**, 2655.
3 M. G. Walter, E. L. Warren, J. R. McKone, S. W. Boettcher, Q. Mi, E. A. Santori and N. S. Lewis, *Chem. Rev.*, 2010, **110**, 6446.
4 A. Kudo and Y. Miseki, *Chem. Soc. Rev.*, 2009, **38**, 253.
5 A. Fujishima and K. Honda, *Nature*, 1972, **238**, 37.
6 T. Hisatomi, T. Minegishi and K. Domen, *Bull. Chem. Soc. Jpn.*, 2012, **85**, 647.
7 Z. Chen, T. F. Jaramillo, T. G. Deutsch, A. Kleiman-Shwarsctein, A. J. Forman, N. Gaillard, R. Garland, K. Takanabe, C. Heske, M. Sunkara, E. W. McFarland, K. Domen, E. L. Miller, J. A. Turner and H. N. Dinh, *J. Mater. Res.*, 2010, **25**, 3.
8 K. Maeda, *ACS Catal.*, 2013, **3**, 1486.
9 K. Maeda and K. Domen, *J. Phys. Chem. C*, 2007, **111**, 7851.
10 Y. Moriya, T. Takata and K. Domen, *Coord. Chem. Rev.*, 2013, **257**, 1957.
11 K. Takanabe and K. Domen, *ChemCatChem*, 2012, **4**, 1485.
12 K. Sivula, F. Le Formal and M. Grätzel, *ChemSusChem*, 2011, **4**, 432.
13 Z. Li, W. Luo, M. Zhang, J. Feng and Z. Zou, *Energy Environ. Sci.*, 2013, **6**, 347.
14 F. E. Osterloh, *Chem. Soc. Rev.*, 2013, **42**, 2294.
15 K. Sivula, *J. Phys. Chem. Lett.*, 2013, **4**, 1624.
16 Y. Sasaki, H. Nemoto, K. Saito and A. Kudo, *J. Phys. Chem. C*, 2009, **113**, 17536.
17 S. S. K. Ma, K. Maeda, T. Hisatomi, M. Tabata, A. Kudo and K. Domen, *Chem.–Eur. J.*, 2013, **19**, 7480.
18 Y. Sasaki, H. Kato and A. Kudo, *J. Am. Chem. Soc.*, 2013, **135**, 5441.
19 M. Moriya, T. Minegishi, H. Kumagai, M. Katayama, J. Kubota and K. Domen, *J. Am. Chem. Soc.*, 2013, **135**, 3733.
20 G. Ma, T. Minegishi, D. Yokoyama, J. Kubota and K. Domen, *Chem. Phys. Lett.*, 2011, **501**, 619.
21 D. Yokoyama, T. Minegishi, K. Jimbo, T. Hisatomi, G. Ma, M. Katayama, J. Kubota, H. Katagiri and K. Domen, *Appl. Phys. Express*, 2010, **3**, 101202.
22 W. Chun, A. Ishikawa, H. Fujisawa, T. Takata, J. N. Kondo, M. Hara, M. Kawai, Y. Matsumoto and K. Domen, *J. Phys. Chem. B*, 2003, **107**, 1798.
23 I. Rahinov, N. Ditzian, A. Goldman and S. Cheskis, *Appl. Phys. B: Lasers Opt.*, 2003, **77**, 541.
24 M. Katsura, *J. Alloys Compd.*, 1982, **182**, 91.
25 A. Ishikawa, Y. Yamada, T. Takata, J. N. Kondo, M. Hara, H. Kobayashi and K. Domen, *Chem. Mater.*, 2003, **15**, 4442.
26 M. Moriya, T. Minegishi, H. Kumagai, M. Katayama, J. Kubota and K. Domen, *J. Am. Chem. Soc.*, 2013, **135**, 3733.
27 K. Maeda, K. Teramura, H. Masuda, T. Takata, N. Saito, Y. Inoue and K. Domen, *J. Phys. Chem. B*, 2006, **110**, 13107.
28 K. Maeda, K. Teramura, D. Lu, N. Saito, Y. Inoue and K. Domen, *Angew. Chem., Int. Ed.*, 2006, **45**, 7806.
29 K. Maeda, H. Hashiguchi, H. Masuda, R. Abe and K. Domen, *J. Phys. Chem. C*, 2008, **112**, 3447.
30 H. Dotan, K. Sivula, M. Grätzel, A. Rothschild and S. C. Warren, *Energy Environ. Sci.*, 2011, **4**, 958.
31 B. Klahr, S. Gimenez, F. Fabregat-Santiago, J. Bisquert and T. W. Hamann, *Energy Environ. Sci.*, 2012, **5**, 7626.
32 H. Kato, K. Asakura and A. Kudo, *J. Am. Chem. Soc.*, 2003, **125**, 3082.
33 Y. Sakata, Y. Matsuda, T. Nakagawa, R. Yasunaga, H. Imamura and K. Teramura, *ChemSusChem*, 2011, **4**, 181.
34 A. Yamakata, T. Ishibashi, H. Kato, A. Kudo and H. Onishi, *J. Phys. Chem. B*, 2003, **107**, 14383.

 This journal is © The Royal Society of Chemistry 2014

Published on 13 January 2014. Downloaded by Indian Institute of Technology Chennai on 07/02/2017 06:22:37.

35 M. Yoshida, A. Yamakata, K. Takanabe, J. Kubota, M. Osawa and K. Domen, *J. Am. Chem. Soc.*, 2009, **131**, 13218.
36 K. Maeda, D. Lu and K. Domen, *Chem.–Eur. J.*, 2013, **19**, 4986.
37 K. Maeda, A. Xiong, T. Yoshinaga, T. Ikeda, N. Sakamoto, T. Hisatomi, M. Takashima, D. Lu, M. Kanehara, T. Setoyama, T. Teranishi and K. Domen, *Angew. Chem., Int. Ed.*, 2010, **49**, 4096.
38 A. Xiong, T. Yoshinaga, T. Ikeda, M. Takashima, T. Hisatomi, K. Maeda, T. Setoyama, T. Teranishi and K. Domen, *Eur. J. Inorg. Chem.*, DOI: 10.1002/ejic.201300439.
39 T. Ohno, L. Bai, T. Hisatomi, K. Maeda and K. Domen, *J. Am. Chem. Soc.*, 2012, **134**, 8254.
40 K. Maeda, M. Higashi, D. Lu, R. Abe and K. Domen, *J. Am. Chem. Soc.*, 2010, **132**, 5858.
41 M. Higashi, R. Abe, T. Takata and K. Domen, *Chem. Mater.*, 2009, **21**, 1543.
42 F. Zhang, A. Yamakata, K. Maeda, Y. Moriya, T. Takata, J. Kubota, K. Teshima, S. Oishi and K. Domen, *J. Am. Chem. Soc.*, 2012, **134**, 8348.
43 S. S. K. Ma, T. Hisatomi, K. Maeda, Y. Moriya and K. Domen, *J. Am. Chem. Soc.*, 2012, **134**, 19993.
44 R. Li, Z. Chen, W. Zhao, F. Zhang, K. Maeda, B. Huang, S. Shen, K. Domen and C. Li, *J. Phys. Chem. C*, 2013, **117**, 376.
45 T. Minegishi, N. Nishimura, J. Kubota and K. Domen, *Chem. Sci.*, 2013, **4**, 1120.
46 M. Higashi, K. Domen and R. Abe, *Energy Environ. Sci.*, 2011, **4**, 4138.
47 Y. Li, T. Takata, D. Cha, K. Takanabe, T. Minegishi, J. Kubota and K. Domen, *Adv. Mater.*, 2013, **25**, 125.
48 M. W. Kanan and D. G. Nocera, *Science*, 2008, **321**, 1072.
49 E.-S. Kim, N. Nishimura, G. Magesh, J.-Y. Kim, J.-W. Jang, H. Jun, J. Kubota, K. Domen and J.-S. Lee, *J. Am. Chem. Soc.*, 2013, **135**, 5375.
50 B. Hinnemann, P. G. Moses, J. Bonde, K. P. Jorgensen, J. H. Nielsen, S. Horch, I. Chorkendorff and J. K. Norskov, *J. Am. Chem. Soc.*, 2005, **127**, 5308.